Bioinspir. Biomim. **7** (2012) 036001 (10pp) doi:10.1088/1748-3182/7/3/036001

Conceptual design of flapping-wing micro air vehicles

J P Whitney and R J Wood

School of Engineering and Applied Sciences, Harvard University, Cambridge, MA 02138, USA

E-mail: rjwood@eecs.harvard.edu

Received 11 October 2011
Accepted for publication 22 February 2012
Published 12 April 2012
Online at stacks.iop.org/BB/7/036001

Abstract

Traditional micro air vehicles (MAVs) are miniature versions of full-scale aircraft from which their design principles closely follow. The first step in aircraft design is the development of a conceptual design, where basic specifications and vehicle size are established. Conceptual design methods do not rely on specific knowledge of the propulsion system, vehicle layout and subsystems; these details are addressed later in the design process. Non-traditional MAV designs based on birds or insects are less common and without well-established conceptual design methods. This paper presents a conceptual design process for hovering flapping-wing vehicles. An energy-based accounting of propulsion and aerodynamics is combined with a one degree-of-freedom dynamic flapping model. Important results include simple analytical expressions for flight endurance and range, predictions for maximum feasible wing size and body mass, and critical design space restrictions resulting from finite wing inertia. A new figure-of-merit for wing structural-inertial efficiency is proposed and used to quantify the performance of real and artificial insect wings. The impact of these results on future flapping-wing MAV designs is discussed in detail.

1. Introduction

Advances in the understanding of insect flight and flapping-wing aerodynamics have prompted several efforts to develop insect-scale flight vehicles. Efforts to date are primarily concerned with the *feasibility* of these devices, rather than the optimization of their performance or the establishment of general design principles. Investigations have focused on maximizing thrust-to-weight or minimizing power consumption. Work in the design and optimization of *individual* vehicle subsystems include efforts to optimize stroke kinematics, wing shape and compliance, transmission efficiency and actuator performance. As a result of these efforts and as evidenced by recent successful prototypes [1–5], development of practical insect-scale flight vehicles is imminent.

As the required technologies mature, there is an increasing need to establish system-level design principles. The design space for these vehicles is very large, and the relationships between design parameters and performance can be complex and counter-intuitive—does minimizing wing loading maximize flight endurance? What impact will the wing size have on the achievable resonant frequency? Is there an optimal flapping frequency? Do larger or smaller vehicles have longer range? Will an optimal design have a large battery mass fraction? Once the feasibility of achieving hover has been addressed, these and many other design questions rise to our attention.

Fixed-wing and rotary-wing aircraft have almost a century of development behind them. Standardized design principles have been developed for every stage of the design cycle, beginning with the *conceptual design* phase: here, gross vehicle parameters are determined, including estimates of vehicle mass, wing/rotor size, propulsion requirements and estimates of the mass fractions of each subsystem. An early step in the conceptual design of a fixed-wing aircraft is called *vehicle sizing* [6]. In this process, vehicle performance requirements are plotted against potential choices for thrust-to-weight ratio (T/W) and wing loading (W/S). The minimum weight vehicle that meets all performance requirements is selected. Variations of this method consider fixed propulsion systems or 'rubber engine' models that scale with vehicle size. Similar methods exist for helicopter design: rotor tip speed is usually chosen by constraints on rotor stall and

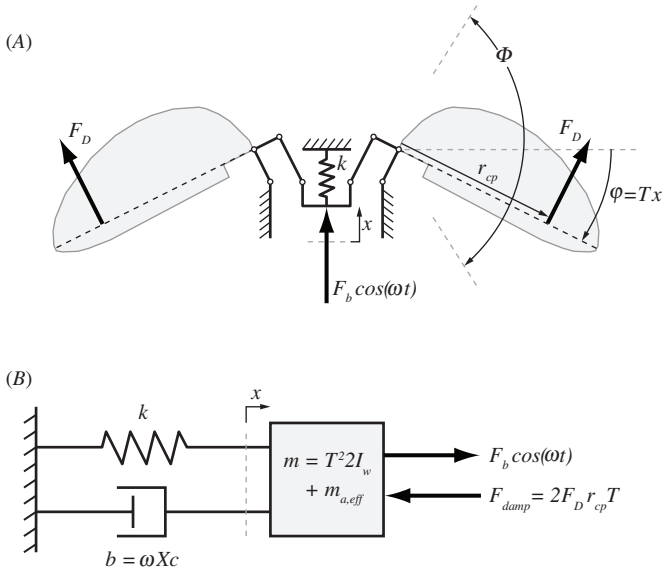

Figure 1. (*A*) Canonical flapping configuration consistent with our model: a single linear actuator drives both wings symmetrically through an (assumed) linear transmission, as viewed normal to the stroke plane. (*B*) Equivalent LP linear model used in our analysis.

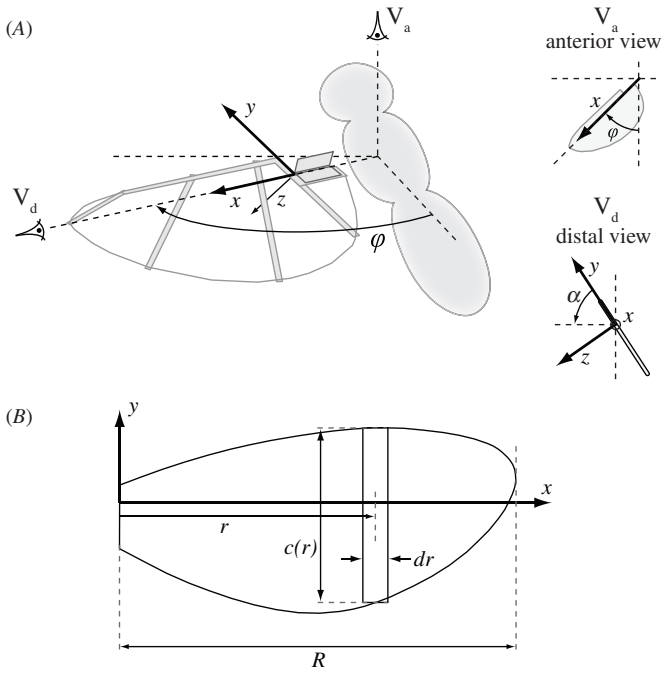

Figure 2. Wings are assumed to flap symmetrically in a horizontal stroke plane, as shown in (*A*). Conventions for flapping angle ϕ and angle-of-attack α are shown. The wing shape is parametrized according to (*B*).

flow compression speeds, autogyration requirements and rotor noise limits [7]. The main rotor is then sized to balance induced and viscous drag losses. In both fixed and rotary vehicle designs, accumulated knowledge of past performance informs the designer 'what works'.

This paper reports our efforts to develop a conceptual design process for flapping-wing vehicles, with a primary focus on hovering flight. Our methods make several simplifying assumptions, but these assumptions are chosen carefully to preserve underlying performance trends. After developing a dynamic model of flapping, actuator and battery mass fractions are determined by energy methods. These sizing methods and the flapping model, combined with derived limits on wing structural-inertial efficiency, determine the range of feasible designs and vehicle performance limits.

2. System dynamics

We will model the actuator-transmission-wing system of a flapping vehicle with an equivalent one degree-of-freedom (DOF) lumped-parameter (LP) linear model, characterized by effective mass, stiffness and damping coefficients. We seek analytical expressions associating these coefficients with a set of independent parameters describing the properties and performance of the actuator, transmission and wings. Figure 1 shows a simplified flapping configuration with a single power actuator driving two wings, and the equivalent translational LP model. We assume that the wings flap symmetrically in a horizontal stroke plane, with peak-to-peak flapping amplitude Φ. The wings are coupled to the drive actuator through a linear, lossless transmission with transmission ratio T, where the time-varying flapping angle $\phi(t)$ and actuator displacement $x(t)$ are related by $\phi = Tx$. The drive actuator is modeled as an idealized force source, characterized by its blocked force F_b and 'static' or 'free' deflection δ_{st}. These values should be taken from operating conditions if dc measurements degrade at high frequencies. The effective mass m is the sum of the actuator effective mass $m_{a,\text{eff}}$ and the effective mass of the wings $2I_wT^2$, where I_w is the mass moment of inertia of a single wing.

With the effective mass m and stiffness $k = F_b/\delta_{st}$ in hand, we only need the damping coefficient b to complete our LP model. Damping results from aerodynamic drag, labeled F_D in figure 1, acting through the aerodynamic center of pressure at the radial position r_{cp}. To estimate drag, we apply a method of scaling experimental data which borrows elements from the classic blade-element theory of propellers [8]. Our methods are in line with established techniques [9, 10] used in the study of insect aerodynamics.

The blade-element method begins with the assumption that aerodynamic forces are proportional to the local dynamic pressure. The wing flaps about its base, and we form chordwise strips as shown in figure 2(*B*); each has an instantaneous local velocity $\dot{\phi}r$. The force (lift or drag) developed on each strip is

$$\mathrm{d}F_{\text{aero}} = \underbrace{\tfrac{1}{2}\rho\dot{\phi}^2r^2}_{p_{\text{dyn}}}\underbrace{C_F(\alpha)}_{C_F}\underbrace{c(r)\mathrm{d}r}_{\mathrm{d}S}, \tag{1}$$

where ρ is the air density, C_F is the force coefficient (a function of angle-of-attack α), and r and c are the radial position and chord, as shown in figure 2. We do not account for local variation of α resulting from induced flow—as commonly done in helicopter or propeller analysis—due to the irregular and highly three-dimensional nature of insect-wing flows.

A simple radial integration leads to an expression for the *instantaneous* lift

$$F_L = \frac{1}{2}\rho\dot{\phi}^2 C_L(\alpha)\bar{c}R^3 \underbrace{\int_0^1 \left(\hat{r}\right)^2 \hat{c}(\hat{r})\,\mathrm{d}\hat{r}}_{\equiv \hat{r}_2^2}, \tag{2}$$

where $\hat{r} = r/R$ and $\bar{c} = A_w/R$. Parameters R, A_w and $\bar{c}$ are the wing radius, area and mean chord. We define the wing aspect ratio[1] $\mathcal{AR} = R/\bar{c}$. The parameter $\hat{r}_2$ is the second wing shape moment as defined by Ellington [11]. We call the net vertical aerodynamic force 'lift'—sometimes called 'thrust'. This equation also gives the instantaneous drag force by simply replacing $C_L(\alpha)$ with $C_D(\alpha)$. Lift and drag coefficients exhibit an experimentally determined variation with angle-of-attack

$$C_L(\alpha) = C_{L_{\max}} \sin(2\alpha),$$
$$C_D(\alpha) = \left(\frac{C_{D_{\max}} + C_{D_0}}{2}\right) - \left(\frac{C_{D_{\max}} - C_{D_0}}{2}\right)\cos(2\alpha). \tag{3}$$

The constant coefficients are determined by experiment. The original coefficients measured by Dickinson in the classic 'robofly' experiment [9] are $C_{L_{\max}} = 1.8$, $C_{D_0} = 0.4$ and $C_{D_{\max}} = 3.4$, measured at a Reynolds number (Re) near 200. Subsequent testing found little variation up to $Re = 10\,000$ [10].

The damping force seen by the actuator during symmetric flapping is twice the drag of one wing, reflected through the transmission

$$F_{\text{damp}} = 2F_D\hat{r}_{cp}RT, \tag{4}$$

where $\hat{r}_{cp}$ is the non-dimensional radial position of the center of pressure ($\hat{r}_{cp} = r_{cp}/R$). For a linear model, the damping force must be proportional to $\dot{\phi}$, but we see in (2) that there is a $\dot{\phi}^2$ dependence. We replace the quadratic term $\dot{\phi}^2$ with $\dot{\phi}_0\dot{\phi}$, where $\dot{\phi}_0$ is the angular velocity at mid-stroke ($\phi = 0$). This 'secant' approximation is a standard way to cope with a quadratic damping term [12].

Sinusoidal excitation, $F_b\cos(\omega t)$, results in a displacement $X\cos(\omega t - \phi_p)$, where X is the amplitude of linear translation, with phase ϕ_p. Using $\dot{\phi} = T\dot{x}$ and $\dot{\phi}_0 = \omega X T$ we find that $F_{\text{damp}} = \omega X c\dot{x}$ and $b = \omega X c$, where

$$c = T^3\rho\widetilde{C}_D\frac{R^5}{\mathcal{AR}}\hat{r}_2^2\hat{r}_{cp}. \tag{5}$$

Note that the damping coefficient b is a parametric function of the solution amplitude and frequency. Since it does not depend on x—only the parameters X and ω—the LP model is still linear. Parametric dependence of b ensures that the correct value of $\dot{\phi}_0$ is used in the approximation for different flapping amplitudes and frequencies.

Since c must be constant, $C_D(\alpha)$ has been replaced with $\widetilde{C}_D \equiv C_D(\alpha_0)$, where α_0 is the angle-of-attack at midstroke. Since C_D is fixed to the midstroke value, we expect errors in F_{damp} away from $\phi = 0$. In figure 3, the actual drag, computed using (4) for sinusoidal flapping and rotation, is compared against the secant approximation (dashed) for a range of values of α_0. Note how the faults of fixed C_D are offset by our previous fault in assuming $\dot{\phi}^2 \to \dot{\phi}_0\dot{\phi}$, particularly for $\alpha_0 = 35^\circ$ and

[1] Be careful; some authors define aspect ratio as $\mathcal{AR} = 2R/\bar{c}$.

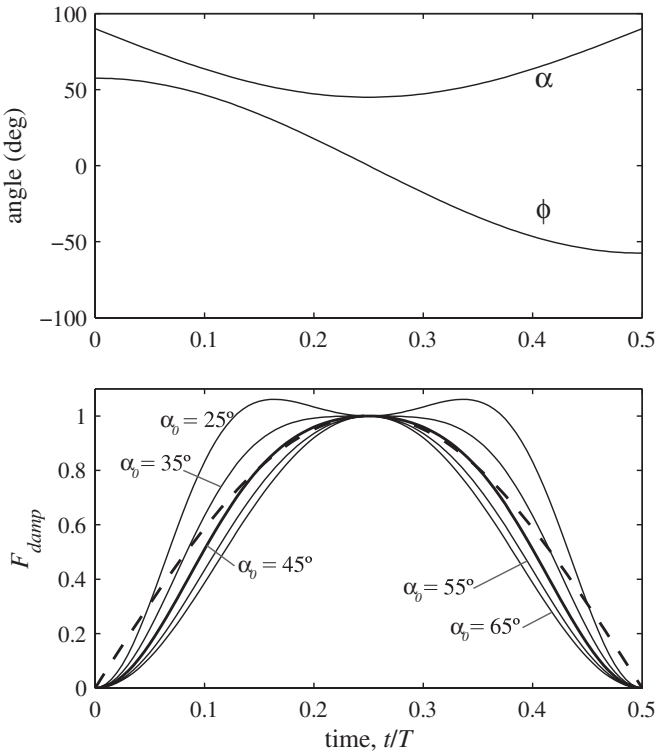

Figure 3. Our conceptual design model assumes sinusoidal flapping and symmetric sinusoidal wing pitching. One-half of a flapping period is plotted, with $\Phi = 115^\circ$ and $\alpha_0 = 45^\circ$. In the lower plot, damping force (arbitrary units) due to drag (solid) is compared with the linear damping force (dashed) obtained with the secant approximation ($\dot{\phi}^2 \to \dot{\phi}_0\dot{\phi}$ and $C_D(\alpha) \to C_D(\alpha_0)$).

$\alpha_0 = 45^\circ$. Away from midstroke we underestimate α (drag prediction low) and overestimate $\dot{\phi}^2$ (drag prediction high). For high wing pitching (small α_0), a significant underprediction of drag levels occurs away from $\phi = 0$. With less pitching (α_0 large), the velocity error dominates, and drag is over-predicted.

We now have analytical expressions for all the coefficients in our LP model:

$$m\ddot{x} + \underbrace{\omega X c}_{\text{'b'}}\dot{x} + kx = F_b\cos(\omega t). \tag{6}$$

The solution is computed using the usual methods, giving

$$\hat{X} = \frac{q^2}{r^2}\left[-\frac{(1-r^2)^2}{2} + \sqrt{\frac{(1-r^2)^4}{4} + \frac{r^4}{q^4}}\right]^{1/2}, \tag{7}$$

where $\hat{X}$ is X/δ_{st} and $r = \omega/\omega_n$, with $\omega_n = \sqrt{k/m}$ the natural frequency. The constant q is defined to be

$$q = \sqrt{\frac{mk}{cF_b}} = \sqrt{\frac{m}{c\delta_{st}}}. \tag{8}$$

We assume hereafter that flapping in hover is designed to occur at the natural frequency ω_n, unburdening the actuator from the task of storing and returning negative power. At $r = 1$, $\hat{X} = q$; thus, q is, by one common definition, the quality factor for this system.

Experiments show that a linear LP model captures the primary resonance of symmetric-flapping insect-scale MAVs

[13]; high frequency behavior resulting from structural modes, nonlinear harmonics and rotational dynamics are not captured.

3. Energetics of hovering

With a model and solution for the dynamics of flapping, we can begin our conceptual design. For a vehicle of a given wing radius R and weight W, we size the actuator by first determining the required blocked force. At the natural frequency, $\hat{X} = q$; when combined with (8), we find

$$F_b = c\omega_n^2 X^2. \tag{9}$$

Note that we can easily transform any expression into its rotational equivalent; here, $F_b = c\omega_n^2 \Phi^2/(2T)^2$. We define the total and static total flapping angles (peak-to-peak) $\Phi \equiv 2TX$ and $\Phi_{st} \equiv 2T\delta_{st}$. To determine the required flapping frequency, we employ the constraint that at hover, $W = 2L$, where W is the total vehicle weight and L is the stroke-averaged lift (thrust) generated by each wing, defined by our conventions as the net vertical aerodynamic force. Substitute (3) into (2) and take the average over one half-period:

$$L = \frac{1}{2}\rho \frac{R^4}{\mathcal{R}} \hat{r}_2^2 \frac{1}{\pi} \int_0^\pi C_{L_{\max}} \sin(2\alpha(s))\, \dot{\phi}_0^2 \cos^2(s)\, \mathrm{d}s. \tag{10}$$

This yields

$$L = \frac{1}{2}\rho \frac{R^4}{\mathcal{R}} \hat{r}_2^2 \frac{1}{2} \widetilde{C}_L \omega^2 T^2 X^2, \tag{11}$$

where we have defined a mean lift coefficient

$$\widetilde{C}_L \equiv C_{L_{\max}} \frac{2}{\pi} \int_0^\pi \sin(2\alpha(s)) \cos^2(s)\, \mathrm{d}s. \tag{12}$$

We do not incorporate the factor of 1/2 seen leading $\widetilde{C}_L$ throughout the paper because it represents the $\cos^2(\omega t)$ reduction in lift that results from sinusoidal flapping. If we assume that wing pitching is also sinusoidal, then $\widetilde{C}_L = 0.94 C_{L_{\max}}$ for the case $\alpha_0 = 45^\circ$; the reduction in effective C_L is largely due to the sinusoidal flapping profile and not wing pitching.

We substitute $L = W/2$ into (11) and rearrange to find the angular flapping frequency required to maintain steady hover

$$\omega_n = \frac{1}{\hat{r}_2 R^2 \frac{1}{2}\Phi} \sqrt{\frac{\mathcal{R}W}{\frac{1}{2}\widetilde{C}_L \rho}}. \tag{13}$$

After substituting (5) and (13) into (9), we obtain the required blocked force

$$F_b = TW \frac{\widetilde{C}_D}{\frac{1}{2}\widetilde{C}_L} \hat{r}_{cp} R. \tag{14}$$

This simple result makes sense intuitively; the blocked force that the actuator must supply is proportional to the mean drag force, which is simply the vehicle weight divided by L/D. The quantity $T\hat{r}_{cp}R$ represents magnification of the drag force through the transmission. In the wing frame, the blocked torque is $Q_b = F_b/T$.

3.1. Sizing the actuator

To develop a mass budget, we divide total vehicle mass m_t into $m_t = m_p + m_b + m_a$, the sum of payload, battery and actuator masses. Here, 'payload' refers to all non-useful mass, including structure, sensors, control actuators, electronics, etc. Any vehicle components which are not the actuator and battery must be accounted for. We also define mass fractions $\mu_p = m_p/m_t$, etc, for these components.

Lacking extensive data from successful designs, we will assume a fixed value for μ_p and decide how to divide the remaining mass budget $1-\mu_p$ between the actuator and battery. The actuator is sized to deliver the required δ_{st} and F_b. Any remaining mass is left to the battery, $\mu_b = 1 - \mu_p - \mu_a$. Under this scheme, we have made μ_a an independent variable; vehicle performance will drive its selection.

To develop a model for actuator mass, we follow the approach of [14], in which the actuator is sized based on the energy it must deliver each flapping period and the energy density S_a (i.e. J kg^{-1}) characteristic to actuators of its type. For a linear bimorph actuator, this balance is given by

$$m_a S_a = F_b \delta_{st}. \tag{15}$$

If the actuator requires power electronics or amplifier circuitry, then the mass of these components must be accounted for by including them in μ_p or by reducing S_a.

It is very important to clarify that with this expression we are assuming a type of actuator in which the actuation frequency and the flapping frequency are required to be the same. This includes piezoelectric, electrostatic, SMA, EAP and other linear[2] strain-based actuators. Pneumatic, chemical and insect flight muscles are other examples. The only actuators that do not qualify are rotary-type (motors) which can use a gearbox to decouple the actuation frequency from the flapping frequency. The major weakness of linear actuators is that their power density will drop as flapping frequency drops, while a motor can maintain peak power output and power density with a gearbox.

If a motor is used, the designer might consider a helicopter MAV over a flapping-wing MAV, especially for larger vehicles. There is some indication that revolving wings outperform flapping wings in hover [10], but in practice, the superiority of either approach has not been demonstrated conclusively for gram-scale and sub-gram MAVs. Since helicopter design is not the focus of this paper, we will primarily consider linear actuators, which are not appropriate for helicopter configurations.

Returning to (15), we substitute (14) to obtain

$$\mu_a = \frac{g}{S_a} \frac{\widetilde{C}_D}{\widetilde{C}_L} \hat{r}_{cp} R \Phi_{st}. \tag{16}$$

Based on this relationship, μ_a is no longer an independent design parameter—its value is set when the designer selects R. Note that μ_a does not depend on vehicle weight, but increases linearly with R. This means that for R large enough, no feasible design is possible; as R increases, μ_a grows until $\mu_a = 1-\mu_p$, consuming all available vehicle mass and leaving no room for

[2] Here 'linear' refers to 'action along a straight line', not linearity of an actuator's input–output relationship.

a battery. This critical wing radius R_{crit} sets an upper bound on the size of the flapping vehicle, independent of vehicle mass,

$$R_{\text{crit}} = \frac{(1-\mu_p)}{\Phi_{st}\hat{r}_{cp}}\frac{\widetilde{C}_L}{\widetilde{C}_D}\frac{S_a}{g}, \tag{17}$$

and thus the actuator mass fraction becomes

$$\mu_a = (1-\mu_p)\frac{R}{R_{\text{crit}}}. \tag{18}$$

There is a limit to how small μ_p can be reduced and L/D maximized; R_{crit} depends primarily on the energy density of the actuator technology. To get an idea of the magnitude of R_{crit}, we can make a few rough assumptions, namely $\mu_p = 0.25$, $\hat{r}_{cp} = 0.6$; this value is representative of typical insect wings [11]; sinusoidal flapping with $\Phi = \Phi_{st} = 115^\circ$ and symmetric sinusoidal wing pitching with $\alpha_0 = 45^\circ$, which yields $\widetilde{C}_L = 1.8$ and $\widetilde{C}_D = 1.9$ from the robofly coefficients and equations (3) and (12); $S_a = 1.5\ \text{J kg}^{-1}$: this value is chosen because it is representative of both insect flight muscle [15] and piezoelectric bimorph actuators [16]. With these numbers (on Earth, $g = 9.8\text{m s}^{-2}$) we obtain $R_{\text{crit}} = 91$ mm. With less payload, better aerodynamic efficiency or higher actuator energy density, larger-winged vehicles are possible.

For this example, we have chosen $q = 1$ ($\Phi = \Phi_{st}$). It appears that a design with $q > 1$ (Φ held constant) will reduce actuator mass and allow designs with larger wings. Whether this is true or not depends on the details of the actuator. For example, piezoelectric actuators are typically strain limited, not field limited, so raising q results in an equivalent reduction of S_a. You can reduce Φ and Φ_{st} both, maintaining $q = 1$, but experiments have shown that reducing flapping amplitude is aerodynamically inefficient. The issue of high-q designs is complex and demands independent attention.

3.2. Flight endurance

We know the required actuator mass fraction, but which R and W do we pick? Answering this requires a performance goal. We start by identifying designs that maximize flight endurance, and later address flight speed and range. Endurance is a good starting point because it speaks directly to the feasibility of a hovering MAV. The expression for hover endurance is simply

$$t_f = \frac{S_b m_b}{P/\eta}, \tag{19}$$

where S_b is the battery energy density, η is the electrical-to-mechanical efficiency of the actuator and associated power electronics, and P is the mechanical power consumed in flapping the wings. From our dynamic model of flapping, the expression for power consumption at $r = 1$ is

$$P_n = \frac{1}{2}F_b\omega_n X. \tag{20}$$

Substituting F_b and ω_n using (14) and (13) gives

$$\frac{P_n}{W} = \sqrt{2}\frac{\widetilde{C}_D}{\widetilde{C}_L^{3/2}}\frac{\hat{r}_{cp}}{\hat{r}_2}\sqrt{\frac{\mathcal{A}W}{\rho R^2}}. \tag{21}$$

This expression is ubiquitous in aircraft design—nearly identical forms exist for airplanes and rotorcraft: P/W is proportional to the square root of *wing loading* or *disk loading*, defined as W/S, where S is an airplane's total wing area or the area swept by a helicopter's main rotor. Since t_f is proportional to W/P_n, it is clear that minimizing wing loading is critical to maximizing flight endurance. After substitution, we obtain the following expression for flight endurance:

$$t_f = \frac{\sqrt{2}}{2}\eta\frac{S_b}{g}\frac{(1-\mu_p)}{\sqrt{W}}\frac{\widetilde{C}_L^{3/2}}{\widetilde{C}_D}\frac{\hat{r}_2}{\hat{r}_{cp}}\sqrt{\frac{\rho}{\mathcal{A}}}\,R\left(1-\frac{R}{R_{\text{crit}}}\right). \tag{22}$$

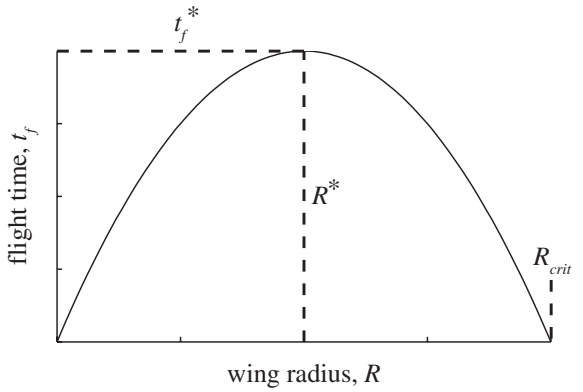

Figure 4. For a given vehicle weight, flight endurance depends quadratically on wing length. When $R = R_{\text{crit}}$, $\mu_a = 1 - \mu_p$, leaving no room for a battery, resulting in a flight time of zero. Maximum flight time t_f^* occurs at $R^* = R_{\text{crit}}/2$.

The dependence of flight endurance on wing radius is illustrated in figure 4. For a wing radius $R^* = R_{\text{crit}}/2$, flight endurance is maximized. This quadratic dependence on R results from two conflicting requirements: minimizing R minimizes μ_a, increasing available battery energy; maximizing R minimizes wing loading, reducing the power required to hover. When $R = R^*$, actuator and battery mass fractions are identical,

$$\mu_a^* = \mu_b^* = \frac{1-\mu_p}{2}, \tag{23}$$

and the expression for maximum flight endurance is

$$t_f^* = \frac{\sqrt{2}}{8}\eta\frac{S_a}{g}\frac{S_b}{g}\frac{(1-\mu_p)^2}{\sqrt{W}}\frac{\widetilde{C}_L^{5/2}}{\widetilde{C}_D^2}\frac{\hat{r}_2}{\hat{r}_{cp}^2}\sqrt{\frac{\rho}{\mathcal{A}}}\frac{1}{\Phi_{st}}. \tag{24}$$

Why is there an inescapable reduction in t_f as W increases? Flight time is inversely proportional to P/W. Note from (21) that maintaining P/W while increasing W requires holding the wing loading constant; if we increase W, a concomitant increase in R^2 is required. Increasing R, however, is not possible; when raised above R_{crit}, savings from reduced power consumption are more than wiped out by the decrease in flight time resulting from a smaller battery.

With a few more assumptions, we can generate representative flight endurance numbers: we assume $\eta = 10\%$, a figure again in line with piezoelectric actuators and insect flight muscles [16, 15]; $\hat{r}_2 = 0.56$ and $\mathcal{A} = 4$, characteristic values for insect wings [11]; $S_b = 500\ \text{kJ kg}^{-1}$, a typical value for lithium polymer batteries [14]; air density $\rho = 1.2\ \text{kg m}^{-3}$. Our choice for S_b may be optimistic because we do not account for capacity derating during high C-rate discharges.

In figure 5, we plot flight endurance over R and m_t. Flight endurance continues to increase as m_t decreases. Our assumption of constant lift and drag coefficients breaks down

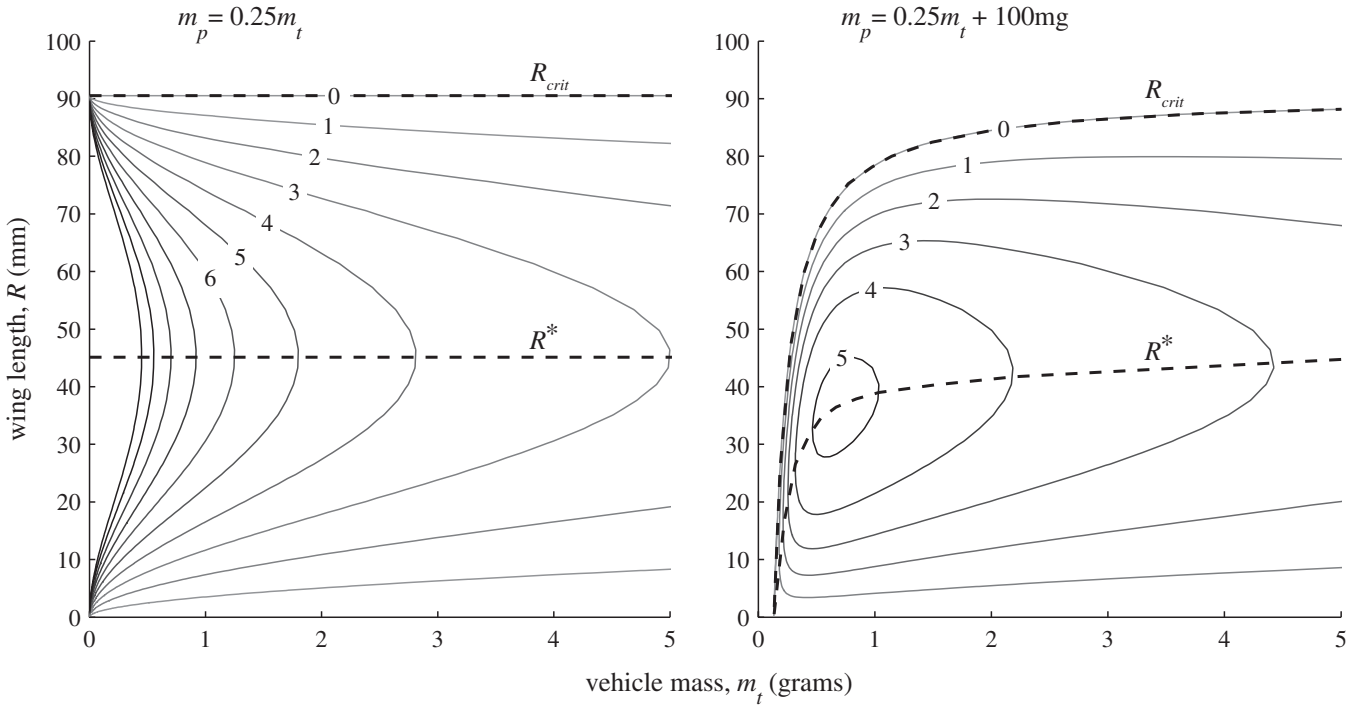

Figure 5. Flight endurance (plotted in minutes) for two different payload mass models. A fixed payload requirement results in a local maximum in flight endurance. Assumed performance values for the battery, actuator and aerodynamics are given in the text.

for Re less than about 100, which corresponds to a vehicle mass of about 1 mg. The variation of other parameters that we have assumed to be constant is likely, such as a probable increase of μ_p as W drops. Fabrication limitations prevent continuous miniaturization of vehicle components. For example, if an additional fixed payload of 100 mg is applied, a local maximum for flight endurance occurs, as shown in figure 5. If variations in C_L, C_D, η, S_a, S_b or μ_p with changes in R and W are known, either from previous designs or more sophisticated models, these results should be modified appropriately.

From these results, it is clear that η are S_b are *critical* parameters, with a great potential to increase flight endurance. Insects are fortunate to carry carbohydrate or fat energy stores with approximately 50 times the energy density of lithium polymer batteries. Increasing the actuator energy density S_a will increase flight time, but large improvements in S_a present diminishing returns unless the designer is willing to increase R to follow resulting increases in R^*. We will see shortly that increasing R negatively impacts flight velocity and range.

It is tempting to use these results to optimize wing shapes through variation of $\hat{r}_{cp}$, $\hat{r}_2$ and $\mathcal{AR}$. Low aspect ratios, for a fixed R, decrease wing loading by increasing wing area. However, low $\mathcal{AR}$ wings may suffer reduced lift and drag coefficients from increased tip losses and a reduction in chord-normalized flapping amplitude. Additionally, our simplified estimates of lift and drag do not account for induced flow effects and their dependence on wing size and shape. Detailed optimization of wing shape and flapping kinematics are second-order effects to be investigated experimentally at a later design stage.

3.3. Flight speed and range

A simple way to predict flight speeds uses the *advance ratio*, a non-dimensional parameter, J, defined as the ratio between forward flight speed V and the mean wingtip velocity

$$J = \frac{V}{2\Phi f R}. \tag{25}$$

From this expression, we can estimate V by assuming a 'reasonable' cruise value for J. A recent flapping MAV capable of controlled hover and forward flight has a reported advance ratio of 0.5 at top speed [5]. As J approaches and exceeds 1, our in-hover model cannot accurately predict lift and drag; a tilted stroke plane is required to overcome rising parasitic body drag, and the relative velocity from forward flight is non-negligible in modeling wing aerodynamics. These issues will affect our ability to accurately predict power consumption and maximum range. Classically, aircraft and helicopters benefit from a reduction in induced drag as flight speed increases, but this is not universally observed in metabolic data from insects [15]. The following analysis seeks only the basic scaling of vehicle range at small J, assuming power consumption is constant with flight speed. We begin by substituting the flapping frequency (13) into (25) to obtain

$$V = \frac{2J}{\pi \hat{r}_2 R}\sqrt{\frac{\mathcal{AR}W}{\frac{1}{2}\widetilde{C}_{L}\rho}}. \tag{26}$$

Achieving high flight speed implies heavy vehicles with small wings. This trend toward smaller wings conflicts with the prescription for maximum flight endurance, which is to grow the wings until reaching the energy density limits of the

actuator. Using the results for V (26) and t_f (22), an estimate of range $d_{\max}$ is obtained:

$$d_{\max} = \eta \frac{2J}{\pi} \frac{S_b}{g} \frac{\widetilde{C}_L}{\widetilde{C}_D} \frac{1}{\hat{r}_{cp}} \left(1 - \frac{R}{R_{\text{crit}}}\right)(1 - \mu_p). \tag{27}$$

Range is not a function of vehicle weight W; it decreases linearly from a maximum at $R = 0$ (obviously pathological) to zero when $R = R_{\text{crit}}$. An endurance-optimized design achieves half the maximum theoretical range. Since flight endurance depends quadratically on R in the neighborhood of $R_{\text{crit}}/2$, a balanced design (e.g. $R = R_{\text{crit}}/4$) might trade a small endurance penalty (-25%) for a larger gain in range ($+50\%$).

4. Flapping dynamics and wing structural-inertial efficiency

For every R–W combination, there is a unique flapping frequency, given by (13), which ensures $L = W/2$. Actuator stiffness $k = F_b/\delta_{st}$ is also fixed by this combination; wing inertia is then set to achieve the required frequency $\omega_n = \sqrt{k/m}$. Since wing inertia cannot be reduced indefinitely, there may be regions of the design space where hover cannot be achieved. To explore this limitation, we need a predictive model for wing mass moment of inertia I_w as a function of R and W.

Lightening the wings will negatively impact their structural performance. To determine the lightest feasible wings, we must establish a wing stiffness criteria. We model each wing as a beam with the mean cross-sectional area A_c, length R and mean density ρ_w. Under these assumptions, wing inertia I_w scales as

$$I_w \propto \rho_w A_c R^3. \tag{28}$$

Bending stiffness requirements determine A_c. The actual loading and deflection of a wing is very complex; we are only interested in how wing deflection scales with changes in wing length R and vehicle weight W. To assess wing stiffness, we hypothetically clamp the wing at its base and load it at the tip with a force equal to the vehicle weight W, and measure the resulting tip deflection w. The Euler model of beam bending yields

$$w \propto \frac{WR^3}{E_w I_{w,a}}, \tag{29}$$

where E_w is the Young modulus and $I_{w,a}$ is the second moment of area of the beam cross-section. Following Ashby [17], we write the second moment of area as

$$I_{w,a} = I_0 \phi_B^e = \frac{A_c^2}{4\pi} \phi_B^e, \tag{30}$$

where I_0 is the second moment of area of a circle, and ϕ_B^e is the *shape factor* of the beam cross-section. High-efficiency shapes, such as I-beams, have a large shape factor; corrugations in insect wings contribute to a high shape factor. We substitute this expression into (29), substitute the non-dimensional tip deflection $\hat{w} = w/R$, and solve for the cross-sectional area:

$$A_c \propto \frac{\sqrt{W} R}{\sqrt{E_w \phi_B^e \hat{w}}}. \tag{31}$$

Substituting it into (28), we obtain

$$I_w = \frac{\sqrt{W} R^4}{\mathcal{M}_1}, \tag{32}$$

where we have defined

$$\mathcal{M}_1 \equiv \phi_w \frac{\sqrt{E_w}}{\rho_w} \sqrt{\hat{w}}, \tag{33}$$

a performance measure of the wing's structural efficiency, which we seek to maximize. The term ϕ_w is an overall measure of wing structural-inertial efficiency, encompassing ϕ_B^e and efficiency improvements from wing tapering. We recognize $\sqrt{E_w}/\rho_w$ as the classic material selection figure-of-merit for bending stiffness [17]. Permitting more tip deflection (larger $\hat{w}$) reduces the stiffness requirement and allows wings with lower inertia (larger $\mathcal{M}_1$). We cannot easily calculate $\mathcal{M}_1$. This would require detailed knowledge of the shape and mass distribution of the wing, and determination of acceptable tip deflection $\hat{w}$. For a conceptual design, it is much easier to empirically determine $\mathcal{M}_1$ from insect and artificial wing data using (32). If our scaling assumptions are correct, $\mathcal{M}_1$ will show little variation with R and W, as it represents a wing 'technology factor' with respect to inertial and structural efficiency. With a representative value for $\mathcal{M}_1$, we can estimate the minimum achievable wing inertia for each R–W combination.

Insect wing data is a good source for testing the scaling prescribed by (32); using data from reference [11], figure 6 plots $\mathcal{M}_1$, derived from reported values of R, W and I_w. Also included is a carbon fiber artificial wing, as reported in [4]; for this wing, W is set to the maximum lift obtained from a pair of these wings in tethered flight testing. This wing is representative of the 'state-of-the-art' in artificial wing fabrication; the spars are laser-cut unidirectional ultra-high modulus (UHM) carbon fiber prepreg, cured and bonded to a 1.5 μm polyester film. While bending tests have confirmed that these wings are comparable in stiffness to similarly sized natural wings [18], their moment of inertia is higher, yielding low $\mathcal{M}_1$ values (~ 70) relative to most natural insect wings.

This I_w-scaling analysis is one of many plausible schemes. For example, it could be assumed that the wing cross-sectional area scales with R^2 or that wing inertial loads drive bending stiffness criteria; the basic dimensional analysis might predict $I_w \sim WR^2$. We could not, however, find an alternative scaling method with better correspondence to published insect wing data. Figures-of-merit derived from these schemes showed much stronger dependence on R and W. Future work in optimizing wing structural–inertial efficiency may improve our understanding of the scaling of I_w—particularly with respect to artificial wings—but the chosen scaling is adequate for the conceptual design phase.

With an estimate for the minimum achievable I_w, the maximum achievable flapping frequency is $\omega_{\max} = \sqrt{\kappa/(2I_w + m_{a,\text{eff}} T^{-2})}$, where $\kappa = k/T^2$. Comparing this maximum frequency with the required frequency (13), we obtain a *minimum* wing radius

$$R_{\min} = \frac{\Phi_{st} \mathcal{R} \sqrt{W}}{\mathcal{M}_1 \hat{r}_{cp} \hat{r}_2^2 \widetilde{C}_D \rho \frac{1}{4} \Phi^2}, \tag{34}$$

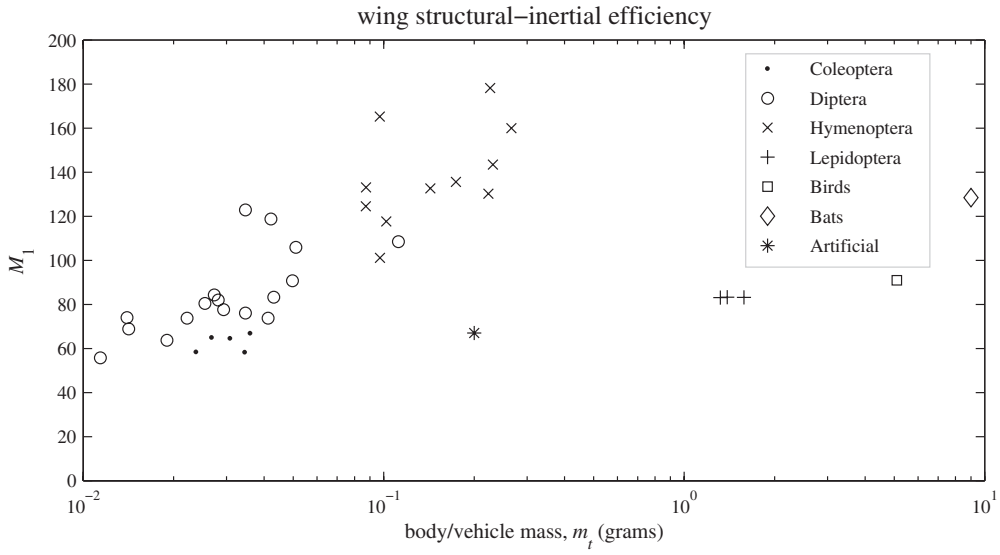

Figure 6. Wing figure-of-merit $\mathcal{M}_1$, as calculated from data in [11], for all nominally two-wing insects with I_w measurements available. The bird (*Amazilia fimbriata fluviatilis*) and bat (*Plecotus auritus*) are both capable of hover. Artificial wing data as reported in [4]. Units of $\mathcal{M}_1$ are $\mathrm{m}^{5/2}\mathrm{kg}^{-1/2}\mathrm{s}^{-1}$.

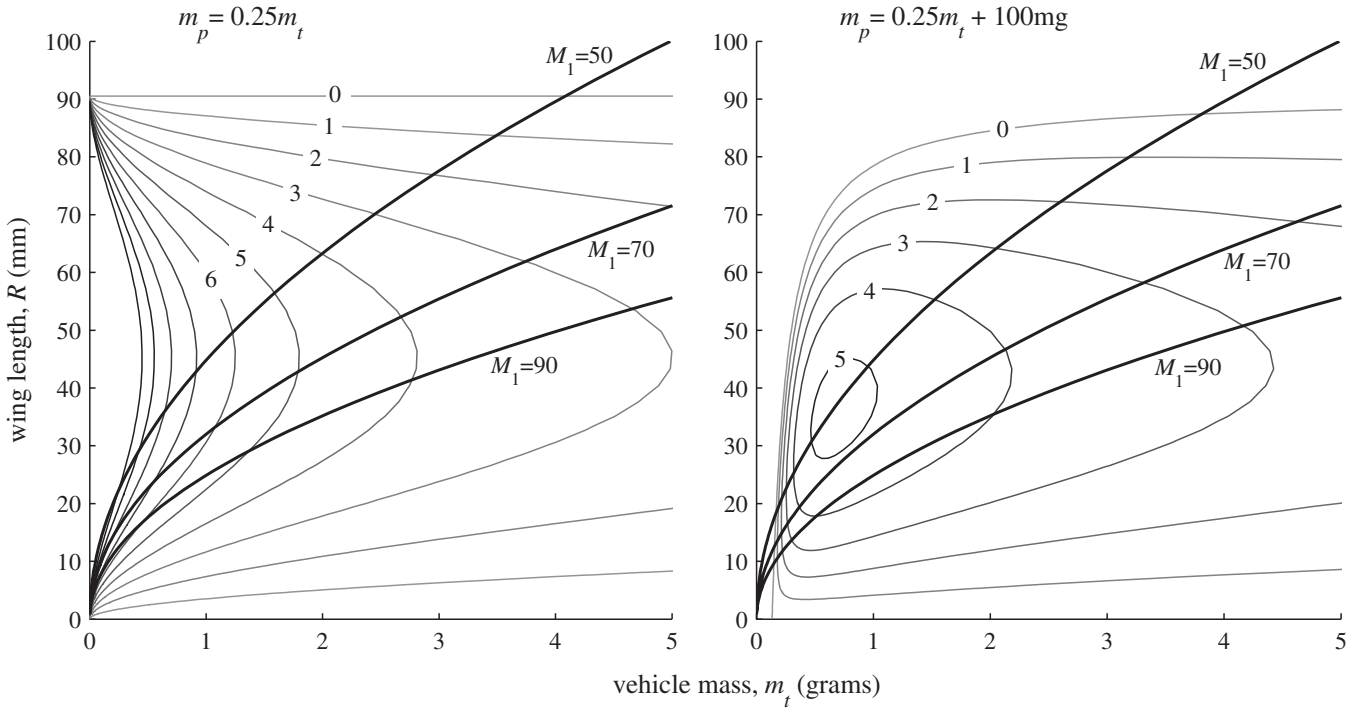

Figure 7. Wing structural–inertial limits for different values of the $\mathcal{M}_1$ figure-of-merit overlay flight endurance results from figure 5. Feasible designs must lie *above* these curves.

where we have assumed that the actuator effective mass is a negligible contributor to overall effective mass. This assumption is tested for high mass vehicles, but achievable transmission ratios—up to 3 rad mm^{-1} in a single-stage flexure-based transmission is feasible without extraordinary effort—are sufficient to reduce actuator effective mass to an insignificant level.

For a given W, designs with a wing radius below $R_{\min}$ cannot flap with a natural frequency high enough to generate sufficient lift to hover. Figure 7 repeats the performance plots of figure 5 with equation (34) overlaid. Feasible designs must lie *above* the inertia-limit curves. For large enough $\mathcal{M}_1$, maximum endurance is not restricted, but fast or heavy long-range designs may still be limited. Where the inertia-limit curve crosses the horizontal line $R = R_{\mathrm{crit}}$, we find a hard upper-bound on the vehicle weight

$$W_{\max} = \left[\mathcal{M}_1(1-\mu_p)\frac{S_a}{g}\frac{\widetilde{C}_L\hat{r}_2^2\rho}{4\mathcal{R}}\left(\frac{\Phi}{\Phi_{st}}\right)^2\right]^2. \qquad (35)$$

Using our previously set representative values, we find maximum vehicle masses of 12 and 20 g for $\mathcal{M}_1 = 70$ and $\mathcal{M}_1 = 90$, respectively. While it is exciting to speculate on the implications of this equation, particularly with respect to establishing an upper bound on, say, hummingbird mass, the quadratic dependence on nearly all parameters, especially S_a, M_1 and μ_p, precludes accurate predictions. On the other hand, the scaling trend is clear: there *are* limits on the maximum feasible weight for hovering MAVs.

The existence of large helicopters appears to contradict this result. We determined $W_{\max}$ by equating the expressions for $R_{\min}$ (34) and R_{crit} (17). However, R_{crit} is only defined for linear-type actuators; if a motor-and-gearbox drive the wings, this expression does not apply. If the actuator is characterized by its power density, S'_a, then the actuator-sizing equation—(15) for linear-type actuators—is replaced with $P_n = S'_a \mu_a m_t$, and the expression for actuator mass fraction becomes

$$\mu_a = \frac{g}{S'_a}\frac{P_n}{W}. \tag{36}$$

There is no upper limit on R; as wing length increases, actuator size and aerodynamic power decrease monotonically. From (36) it is straightforward to re-derive expressions for flight endurance and range. However, previous results for aerodynamic power (21) and flight speed (26) remain the same. Wing inertial-structural limits and the expression for $R_{\min}$ are also unchanged.

5. Discussion and future work

There are several important results worth summarizing. When driven by linear (non-gearbox) actuators, a reduction in flapping frequency decreases actuator power density. This sets up a conflict between minimizing aerodynamic power and maximizing actuator power density. For fixed payload mass fraction, there is a fixed maximum wing length, independent of vehicle mass; endurance-maximizing designs will have a wing length half this maximum. For these designs, the battery mass fraction and actuator mass fraction will always be equal, no matter their respective energy densities. Using a motor and gearbox to drive the wings removes the upper limit on wing size, allowing high-mass designs that are not feasible when using linear actuators.

Wing inertia determines the maximum possible flapping frequency, which sets a lower bound on wing length and an upper bound on flight velocity. These bounds hold for both linear and motor actuators, but for linear actuators, finite wing inertia also leads to a limit on maximum vehicle mass. Physical reasoning and morphological insect data indicate that wing mass moment of inertia scales, roughly, as the product of wing radius to the fourth power and the square root of body/vehicle mass.

Opportunities for improvement and expansion of these models are manifold. If the type of actuator is known, then an improved model of power efficiency can be included. For example, the low efficiency of piezoelectric actuators results primarily from dielectric losses; a loss model can replace the generic efficiency factor used here. If chemical or pneumatic actuators are used, the effect of time-varying mass can be included. Structural models and experimental data can replace the assumption of constant payload mass fraction. Payload models are easily modified to include known masses, such as processing and power electronics, sensors and other fixed payloads.

Our conceptual design does not yet cover the control system. Many different control schemes are under active research, and clear winners have not yet emerged. The designer is forced to complete a detailed control system design before performing vehicle sizing. In time, the performance characteristics of the best control methods will be determined, and these data will provide preliminary mass and power estimates of the control system, allowing sizing and performance calculations to be performed before the detailed design phase.

Past the conceptual design phase, further refinements include detailed selection and modeling of flapping kinematics, transmission design, passive or active wing rotation design, wing testing and planform selection, and design and modeling of a vehicle control architecture; existing research on these topics is extensive.

It would be unwise to draw quantitative conclusions from any numerical results presented in this paper; for different actuator types and battery technologies, there is a large variation in energy density and efficiency—specifications which have a tremendous impact on system performance. In spite of this, the analytical results present clear design trends worthy of examination. MAVs driven by linear actuators are most appropriate for low-mass designs. As vehicle mass drops, there is greater flexibility in selecting wing size and flight endurance rises; fabrication limitations will set the minimum feasible size. As vehicle mass rises, at some point it becomes necessary to switch to motors. The precise cross-over mass—perhaps in the range of a few grams—depends on the efficiency and performance of available motors and linear actuators. Once the switch to motors is made, the designer must consider the advantages and disadvantages of moving to a helicopter design. It is not yet clear if flapping MAVs are faster or more maneuverable than their helicopter counterparts.

Flapping-wing MAVs show promising advantages, especially at the scale of small flying insects. Advances in fabrication and miniaturization continue to expand the feasible design space of these tiny vehicles, but the dependence of vehicle performance on design parameters is not always direct or intuitive. Designs must meet a range of competing performance requirements, such as size, payload, flight endurance and speed. Optimizing indirect quantities, such as power consumption and lift, is an incomplete approach. Traditional aircraft conceptual design methods provide a model for balancing design requirements and optimizing performance. These ideas are easily and powerfully adapted to flapping-wing MAVs; useful not only for current designs, but in efficiently directing future research efforts to improve performance.

Acknowledgments

This work was partially supported by the National Science Foundation (award number CCF-0926148), the Air Force

Office of Scientific Research (award number FA9550-09-1-0156) and the Wyss Institute for Biologically Inspired Engineering. Any opinions, findings and conclusions or recommendations expressed in this material are those of the authors and do not necessarily reflect the views of the National Science Foundation.

References

[1] Fearing R S, Chiang K H, Dickinson M H, Pick M H, Sitti D L and Yan J 2000 Wing transmission for a micromechanical flying insect *Proc. IEEE Int. Conf. Robotics Automation (San Francisco, CA)* pp 1509–16

[2] Pornsin-Sirirak T N, Tai Y C, Ho C M and Keennon M 2001 Microbat: a palm-sized electrically powered ornithopter *Proc. NASA/JPL Workshop on Biomorphic Robotics* pp 14–17

[3] Lentink D, Jongerius S R and Bradshaw N L 2009 The scalable design of flapping micro-air vehicles inspired by insect flight *Flying Insects and Robots* (New York: Springer) pp 185–205

[4] Pérez-Arancibia N O, Ma K Y, Galloway K C, Greenberg J D and Wood R J 2011 First controlled vertical flight of a biologically inspired microrobot *Bioinsp. Biomim.* **6** 036009

[5] Keennon M, Klingebiel K, Won H and Andriukov A 2012 Development of the nano hummingbird: a tailless flapping wing micro air vehicle *50th AIAA Aerospace Sciences Meeting* vol 0588 pp 1–24

[6] Raymer D P 2006 *Aircraft Design: A Conceptual Approach* (Reston, VA: American Institute of Aeronautics and Astronautics)

[7] Leishman J G 2006 *Principles of Helicopter Aerodynamics* (Cambridge: Cambridge University Press)

[8] Glauert H 1935 Airplane propellers *Aerodyn. Theory* **4** 169–360

[9] Dickinson M H, Lehmann F-O and Sane S P 1999 Wing rotation and the aerodynamic basis of insect flight *Science* **284** 1954–60

[10] Lentink D and Dickinson M H 2009 Rotational accelerations stabilize leading edge vortices on revolving fly wings *J. Exp. Biol.* **212** 2705–19

[11] Ellington C P 1984 The aerodynamics of insect flight: II. Morphological parameters *Phil. Trans. R. Soc.* B **305** 17–40

[12] Rao S S 1990 *Mechanical Vibrations* (New York: Addison-Wesley)

[13] Finio B M, Pérez-Arancibia N O and Wood R J 2011 System identification and linear time-invariant modeling of an insect-sized flapping-wing micro air vehicle *IROS: IEEE/RSJ Int. Conf. Intelligent Robots and Systems* pp 1107–14

[14] Karpelson M, Whitney J P, Wei G Y and Wood R J 2010 Energetics of flapping-wing robotic insects: towards autonomous hovering flight *IROS: IEEE/RSJ Int. Conf. on Intelligent Robots and Systems* pp 1630–7

[15] Dudley R 2000 *The Biomechanics of Insect Flight: Form, Function, Evolution* (Princeton, NJ: Princeton University Press)

[16] Wood R J, Steltz E and Fearing R S 2005 Nonlinear performance limits for high energy density piezoelectric bending actuators *ICRA: Proc. 2005 IEEE Int. Conf. on Robotics and Automation* pp 3633–40

[17] Ashby M F 2005 *Materials Selection in Mechanical Design* (Oxford: Butterworth-Heinemann)

[18] Tanaka H, Whitney J P and Wood R J 2011 Effect of flexural and torsional wing flexibility on lift generation in hoverfly flight *Integr. Comp. Biol.* **51** 142